High-Resolution Visualization of Fibrinogen Molecules and Fibrin Fibers with Atomic Force Microscopy

Ivan S. Yermolenko,[†] Valeryi K. Lishko,[†] Tatiana P. Ugarova,[*,†] and Sergei N. Magonov[*,‡]

The Center for Metabolic and Vascular Biology and School of Life Sciences, Arizona State University, Tempe, Arizona 85287, United States, and Agilent Technologies, Chandler, Arizona 85226, United States

Received September 20, 2010; Revised Manuscript Received December 7, 2010

We report an atomic force microscopy (AFM) study of fibrinogen molecules and fibrin fibers with resolution previously achieved only in few electron microscopy images. Not only are all objects triads, but the peripheral D regions are resolved into the two subdomains, apparently corresponding to the βC and γC domains. The conformational analysis of a large population of fibrinogen molecules on mica revealed the two most energetically favorable conformations characterized by bending angles of ~100 and 160 degrees. Computer modeling of the experimental images of fibrinogen molecules showed that the AFM patterns are in good agreement with the molecular dimensions and shapes detected by other methods. Imaging in different environments supports the expected hydration of the fibrinogen molecules in buffer, whereas imaging in humid air suggests the 2D spreading of fibrinogen on mica induced by an adsorbed water layer. Visualization of intact hydrated fibrin fibers showed cross-striations with an axial period of 24.0 ± 1.6 nm, in agreement with a pattern detected earlier with electron microscopy and small-angle X-ray diffraction. However, this order is clearly detected on the surface of thin fibers and becomes less discernible with the fiber's growth. This structural change is consistent with the proposal that thinner fibers are denser than thicker ones, that is, that the molecule packing decreases with the increasing of the fibers' diameter.

Introduction

A physiologically important process of hemostasis is related to the behavior of the fibrinogen molecules and their polymerization into a fibrillar fibrin network resulting in blood clotting. The understanding of this process at different levels of structural organization is essential for diagnosis and treatment of related pathological phenomena such as thrombosis and atherosclerosis. Moreover, fibrinogen adsorbed on the surface of implanted biomaterials may support platelet and leukocyte adhesion and, thus play a critical role in the processes of surface-induced thrombosis and inflammation. Hence, revealing the interactions of fibrinogen with various surfaces has the potential to improve biocompatibility of biomaterials. The extensive structural information about fibrinogen and fibrin has been obtained over the years with electron microscopy and diffraction techniques.[1−7] Visualization of individual fibrinogen molecules adsorbed on mica with TEM led to a model of this 340 kDa molecule as a centrosymmetric linear structure of ~47 nm in length. It consists of three nodules connected by thin α-helical coiled coils of less than 1.5 nm in diameter. The two peripheral D nodules (the D regions) are 6.5 nm in diameter, and the central nodule (the E region) is 5 nm. This architecture represents an assembly of two sets of the polypeptide chains (Aα, Bβ and γ) disulfide-linked together via their N-terminal parts in the central E nodule (Figure 1A). Each connector consists of the three-chained α-helical coiled coils. The C-termini of the Aα chains, called αC, exit the D nodules and extend along the surface of the protein as thin strands toward the E nodule. The D regions are formed by the C-terminal parts of the Bβ and γ chains, which are folded into the βC and γC domains, respectively.

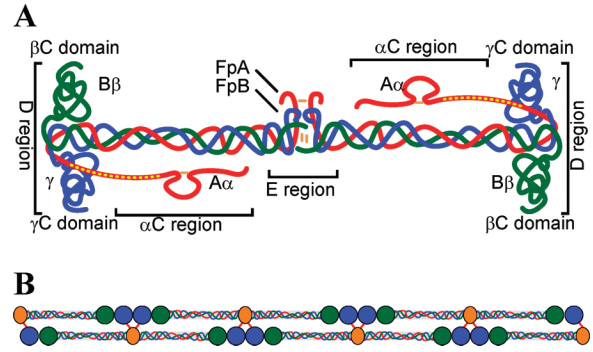

Figure 1. Schematic representation of the fibrinogen molecule and the protofibril. (A) The three chains, Aα, Bβ, and γ in the fibrinogen molecule are shown in red, green, and blue, respectively. FpA and FpB are small fibrinopeptides in the central E region, which are cleaved by thrombin to initiate fibrin polymerization. The peripheral D regions are composed of the βC and γC domains. (B) The half-staggered interactions between individual molecules within a double-stranded protofibril.

Visualization of the individual βC and γC domains has been achieved in several TEM studies[7−10] and is in agreement with the three-dimensional structure of human fibrinogen.[11] The flexible αC regions, which have not been resolved in the crystal structures of fibrinogen, are visible in the shadowed and negatively stained specimens as an extra nodule near the central E region.[12−14]

Structural studies of fibrin polymerization revealed several distinctive features of protofibrils, the early products of polymerization, as well as those of fibrin fibers generated in the latter stages of fibrin formation. The TEM images showed that the formation of twisted two-stranded protofibrils is essentially the primary step of fibrin polymerization.[6,7,15] At later stages, the protofibrils associate laterally, forming the long fibers that

* To whom correspondence should be addressed. E-mail: tatiana.ugarova@asu.edu; sergei_magonov@agilent.com.
[†] Arizona State University.
[‡] Agilent Technologies.

10.1021/bm101122g
Published on Web 12/30/2010

exhibit a regular repeat of 22.5 nm.[15,16] The micrographs of the stained fibrin samples display a narrow stain-receptive band midway between two denser and wider bands whose average distance center to center along the fiber axis is also ~23 nm. This structural order is explained by a half molecule stagger between strands resulting from the interaction between the E nodules within one strand with the peripheral D nodules in the adjacent filament (Figure 1B). Furthermore, there is a strong tendency of striations to align between adjacent fibers in a bundle. It was observed that striations are gradually dissolved into the random particulate structures toward the tapered ends of the fiber. The X-ray diffraction studies of fibrin films and gels have showed the same axial spacing of 22.5 nm.[3,17,18]

The examination of single fibrinogen molecules with atomic force microscopy (AFM) has attracted researchers shortly after the introduction of this technique.[19] The dimension and conformation of the individual fibrinogen molecules were examined on a variety of surfaces, including SiO_2, TiO_2, mica, graphite, glass, organic self-assembled layers, polymers, stainless steel, and other materials.[20−31] Such studies are most relevant to adsorption of fibrinogen from the blood onto biomaterials. Although the resolution of the obtained images varies, the individual trinodular molecules in a linear or a slightly bent shape were observed in the majority of studies. The best resolved nanometer-scale features were assigned to the D and E regions; yet a fine substructure of the outer D nodule has not been reported. Imaging of individual fibrinogen molecules showed the trinodular structures not only in air but also in aqueous conditions.[27,29,32] Nevertheless, despite the general agreement on the overall shape of fibrinogen revealed by AFM, there is a notable difference in the reported relative heights of the D and E regions. Numerous examples have been described in which the surface chemistry may influence the height of adsorbed fibrinogen.[22,27,31,33] However, even after adsorption on the same surface (for example, atomically smooth mica), the images of fibrinogen display a variability of heights.[25−27,34] To explain these differences, the time-dependent unfolding and spreading of adsorbed molecules on the substrate, as well as different imaging environments, have been proposed as a possible cause.[26,27]

Polymerization of fibrin has also been examined with AFM, and the initial stages of fibrin formation in aqueous media or in air on surfaces of graphite and mica have been reported in selected studies.[35−39] The use of supersharp AFM probes allowed visualization of the fine structure of protofibrils and identification of the individual D and E regions assembled along the strand consistent with its double-stranded structure.[38] Yet, the detection of the striated pattern of fibers observed previously by TEM has not been reported.

Despite the broad use of AFM for characterization of materials, the potential of this method, especially for high-resolution imaging of soft materials such as biological objects, is not fully realized. Ongoing instrumental developments, thorough modeling of AFM operation, and accumulating practical experience are the driving forces that will lead to advanced applications. The present study describes the high-resolution AFM visualization of the fibrinogen molecules and fibrin fibers in different environments. In this revisiting of the molecular-scale imaging of the fibrinogen molecules, we addressed the statistically sound visualization of these objects and the related conformation analysis. The interpretation of AFM images was assisted by the use of a theoretical simulator of AFM images that revealed the influence of the geometry of the probe. In the analysis of the fibrin fibers, we focused on the nanoscale details of the surface structures. Particularly, we found that while thin fibers exhibit the periodic surface corrugations with a pitch of 24.0 ± 1.6 nm similar to that which is commonly found in TEM images, the surfaces of thicker fibers are formed of granular structures that lack this order. This is in contrast to a paracrystalline order invariably observed in TEM micrographs of fibers with different sizes. The coexistence of regions with a different structural order is in agreement with a previous proposal that fibrin fibers have an irregular density, being denser in the center than on the outside.[39,40]

Materials and Methods

Sample Preparation. Fibrinogen, depleted of fibronectin and plasminogen, was purchased from Enzyme Research Laboratories (South Bend, IN). The absence of fibronectin was verified by SDS-PAGE and Western blotting using antifibronectin antibodies. To ensure a minimal level of contamination, which is essential for AFM visualization of individual molecules, the double distilled water and phosphate-buffered saline (PBS) were freshly prepared. The fibrinogen concentration in PBS was analyzed by a spectrophotometer and the extinction coefficient 1.506 at 280 nm was used for 1 mg/mL concentration of the protein. For AFM images, the samples of fibrinogen were made by dipping freshly cleaved mica substrates into the fibrinogen solutions (0.1−1.0 μg/mL) for different times at 37 °C. An excess of fibrinogen was removed from the substrate by rinsing it with distilled water followed by drying in a stream of argon gas. Fibrin-monomer was produced by clotting fibrinogen with thrombin and by dissolving the rinsed clot in 0.02 M acetic acid at 4 °C as previously described.[41] Fibrin-monomer differs from fibrinogen by the absence of two small fibrinopeptides A and B and is indistinguishable from fibrinogen by AFM.[37] To produce fibrin fibers, fibrin-monomer was diluted to a final concentration of 0.1 mg/mL with PBS, and after 5 min, a droplet of the solution was placed onto mica. After 60 min at 22 °C in a humid environment to prevent evaporation, a sample was washed with distilled water and dried under a stream of argon gas.

AFM Imaging. An Agilent 5500 (Agilent Technologies, Chandler, AZ) scanning probe microscope, equipped with an environmental chamber, was used in the experiments. The measurements were performed in the oscillatory amplitude modulation (AM) and frequency modulation (FM) modes with commercial Si probes whose stiffness varies in the 0.5−40 N/m range with the softer ones being preferable for imaging of single fibrinogen molecules. The operation at low levels of tip−sample force interactions, which is essential for a nondestructive and high-resolution visualization of these soft objects, was further optimized by using smaller operating amplitudes (1−3 nm). In some cases, the force level was elevated to detect the possible stiffness variations of the objects. The studies of the single molecules and fibrin fibers were carried out with small- and large-scale scanners, respectively. The scanners were calibrated with the 10 and 1 μm gratings as well as with samples of $C_{60}H_{122}$ alkanes on graphite that have 7.5 nm lamellar spacing.[42] The experiments were conducted at ambient conditions and also at high humidity (RH > 90%). The humidity surrounding the sample was made by the injection of several milliliters of water in the microscope environmental chamber and controlled by a humidity meter. The measurements in PBS were made in the oscillatory AM mode with the Si probe (spring constant 1.7 N/m). The probe was driven into oscillation at its resonant frequency (21 kHz) in buffer.

In some experiments, high-density images were collected in which the number of pixels was increased from 512 × 512 to 4096 × 4096. This allowed the visualization of a large colony of fibrinogen molecules in a single image and the off-line statistical analysis of the size and conformation of the individual species by zooming into different locations of the high-density picture. In case of fibrillar structures, such high-density images show not only an overall morphology of the fibrin network at the tens of micrometers scale, but also the fine details of

nanoscale structures of different fibers. The off-line treatment of the AFM images was performed with the PicoView and Gwyddion software packages.

Simulation of AFM Images. The interpretation of AFM images of single fibrinogen molecules was assisted by the computer program that allows a simulation of the images at different levels of the tip−sample forces and for probes with various tip sizes.[43] The computer simulation of AM mode is based on the modeling of the probe motion using an Euler−Bernoulli equation,[43] with consideration of its force interactions with a sample. The Krylov−Bogoliubov−Mitropolsky averaging method[44] was applied to derive asymptotic steady state equations of a controllably oscillating AFM. In this simulation, the tip and sample are represented by assemblies of spheres characterized by their elastic moduli, radii, and relative positions.[43,45] Based on recent crystallographic studies,[11] the geometry of carbon skeleton of the fibrinogen molecule was reconstructed with an open-source Java viewer for chemical structures in 3D (Jmol: www.jmol.org). For computer simulation, the βC and γC domains, as well as the E region and the coiled-coil connectors, were approximated as a number of spheres with specific diameters (Table S1 in the Supporting Information). The dimensions are slightly less than those deducted from TEM, but this underestimation does not substantially influence the results of the image simulations. The flat substrate was approximated by a sphere with a relatively large (infinite) 10 m radius, with a Young modulus of 60 GPa. The probe was approximated by a hard sphere ($E = 100$ GPa) with a radius in the 0.15−60 nm range. The smallest radius corresponds to an ideally sharp probe of atomic size. The regular commercial Si probes have a radius more than 5 nm. The force interactions between the probe and fibrinogen are considered using the Hertz model. The simulation of the AFM topography images was performed for operation in the contact and AM modes.

Results and Discussion

Visualization of Fibrinogen Molecules. Imaging of the fibrinogen molecules was performed on a large variety of samples in air, humid air (RH > 90%), and in buffer. The optimal coverage of the mica surface by single molecules with a large number of individual objects evenly spread on the substrate was obtained at a concentration of 0.6 μg/mL. A large data set for the extraction of statistically valid information was collected. The representative AFM image of fibrinogen adsorbate in air is presented in Figure 2A. It shows a 3.66 × 3.66 μm^2 area where numerous nanoscale objects, as well as few large aggregates, are distributed on the surface. The trinodular molecules of fibrinogen can be easily recognized in Figure 2B, which shows two off-line zoomed pictures of the surface locations boxed in Figure 2A. Among ∼3500 trinodular structures revealed in the image, 333 objects that can be assigned to the single fibrinogen molecules firmly attached to the substrate with all three domains, were selected for analyses. The large objects, which may present molecular aggregates, were not included in these analyses. A variety of conformations can be recognized in the selected molecular colony (Figure 2C). Similar signatures of individual fibrinogen molecules in AFM images have been reported previously,[23,27,37] but without extensive statistical analysis. The histogram of the contour length is presented in Figures 2D. The distribution of the contour length is centered near 46 nm in agreement with the expected length of the fibrinogen molecules. An analysis of the vertical and lateral dimensions of the fibrinogen domains showed that the D regions have a width of 6.8 ± 0.9 nm and a height of 1.1 ± 0.3 nm. The E regions are characterized by a width of 6.4 ± 0.9 nm and a height of 0.7 ± 0.1 nm.

The histogram of the angle between the lines connecting the central and the terminal domains are presented in Figure 2E. Our examination showed that straight structures are rare and, instead, the molecules are bent at different angles. The angle distribution revealed the two most probable conformations of fibrinogen on mica characterized by the bending angles of 106 degrees (Figure 2E and C, middle column) and 157 degrees (Figure 2E and C, right column), which were found in 27 and 59% of the molecules, respectively. A small fraction of the molecules (4%) adopts a triangle-like shape with an angle of ∼60−70 degrees between the D regions (Figure 2C, left column). The bent fibrinogen molecules have been previously detected in images of freeze-dried samples obtained by scanning transmission electron microscopy.[12] Moreover, Mosesson et al.[12] have reported compact folded structures in the freeze-dried samples, which apparently correspond to the triangle-shaped molecules identified in the present study. Molecular flexibility was also evident in negatively stained and rotary shadowed preparations of fibrinogen, as judged by the presence of linear, bent, and compact forms.[2,8,12,15,46] The fact that folded conformations have been detected by various microscopy techniques suggests that the fibrinogen molecules may adopt a range of shapes in solution as well. The availability of completely and partially bent conformations raises an interesting question about the mechanism by which the bent molecules are incorporated into a protofibril. Numerous studies have shown that a majority of fibrin monomers that form long protofibrils are straightened.[6,15,16,47] However, electron microscopy images of short complexes consisting of 3−5 molecules have revealed that the fibrin monomers that are at a stage of docking to the preformed fibrinogen oligomers are in a bent conformation.[6] Furthermore, fibrin monomers seen in the AFM images of short protofobrils reported by Chtcheglova are also bent.[38] Notwithstanding the numerous lines of evidence that indicate a linear structure of fibrin monomers in a protofibril, the possibility that bent molecules exist in solution and then unfold and straighten out upon assembly into protofibrils, or upon removal of fibrinopeptides A and B by thrombin, remains to be addressed.

High-resolution imaging of fibrinogen and visualization of its individual domains is a challenging task in microscopy techniques. In the case of TEM, a grain structure of metal coating limits the resolution. The highest resolution micrographs reported[7,48] were usually used for a schematic presentation of the submolecular fibrinogen structure. For AFM, the probe sharpness and a fine-tuning of the probe-sample force interactions present the main difficulties for high-resolution visualization of the molecular and atomic structures. As with TEM, few AFM images show the fine details of the submolecular structure of the D and E regions. Moreover, recording of the high-resolution images is possible only when the soft probes with the stiffness below 1 N/m are applied; otherwise, the molecules are swept away by a scanning probe when imaging is performed at the submicrometer scales. The area containing a number of separately lying single fibrinogen molecules is shown in Figure 3A. Linear dimensions of these features are consistent with the expected length of the molecule and their trinodular structures are well distinguished. At higher magnification, the submolecular structure of the individual D regions is well resolved (Figure 3B). Eight snapshots of several AFM patterns are presented in Figure 3C. A possible assignment of these features to the D and E regions is indicated with red tracings overlaid on the individual patterns. These contours were constructed based upon the fine molecular features observed previously in the high-resolution TEM images.[7−10,12,13] The best visual fit between the fibrinogen conformation and the observed substructures was achieved by varying the conformation of the connecting

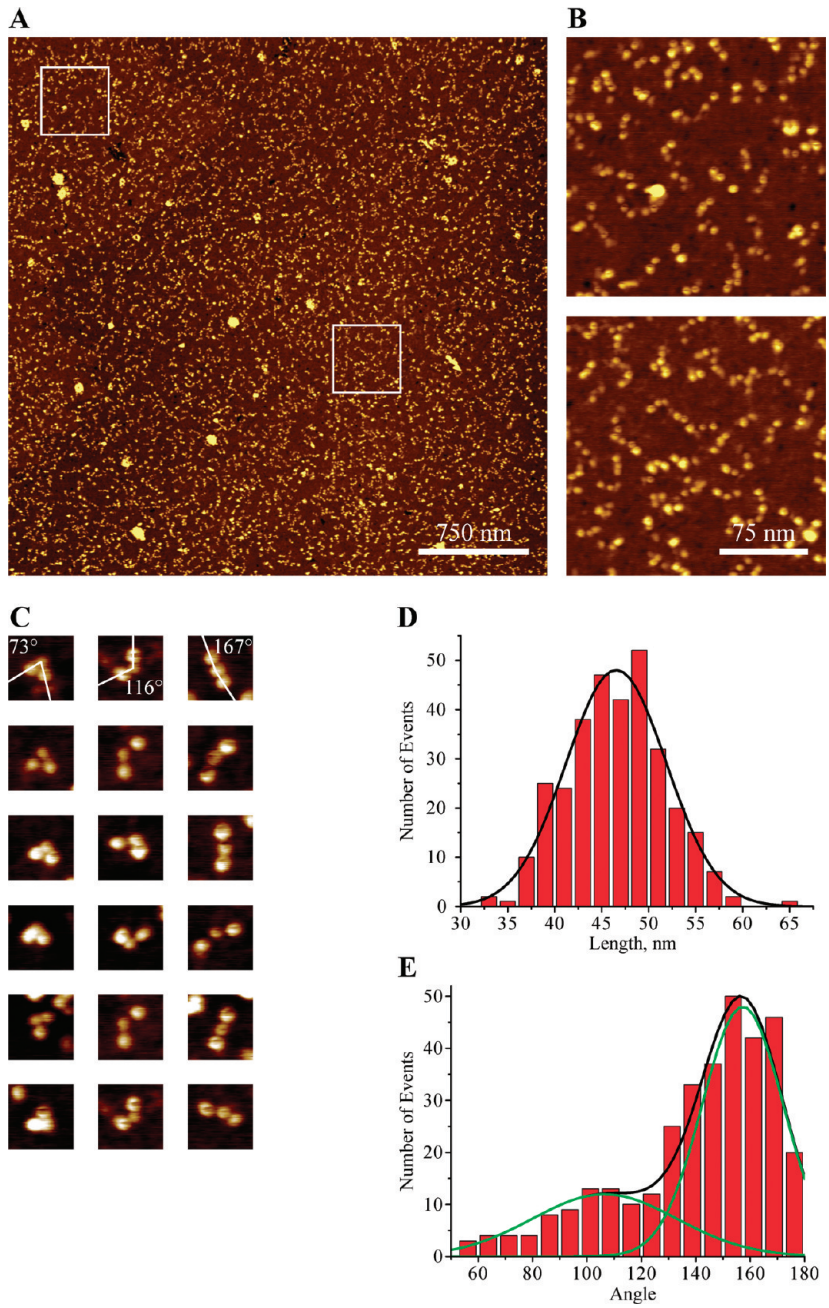

Figure 2. Analyses of the fibrinogen conformation. (A) High-density topography image (4096 × 4096 pixels) of a colony of the fibrinogen molecules that was used in the analyses of the fibrinogen conformation. (B) Representative topography images (512 × 512 pixels) of two locations boxed in panel A. The contrast covers the height corrugations in the range of 0−2 nm in all images. (C) Gallery of the individual fibrinogen molecules revealing a variety of molecular conformations. The histograms show the distribution of the lengths (D) and the angles (E) in fibrinogen molecules. The bending angle was defined as the angle between the middle-point of the outer D domains measured through the middle point of the central E domain.

filaments which link the D and E regions. Although the path of filaments in the images can vary, the lower resolution AFM image will most likely produce a typical trinodular outline. Also shown in Figure 3C and D are the high-contrast patterns of each molecular snapshot which were generated by the removal of the background. They confirm a tentative assignment of the features indicated by red tracings to the domains and connecting filaments. The terminal D regions in several molecules are divided into two subdomains which apparently correspond to the βC and γC domains. Furthermore, several molecules have additional small globules in the vicinity of the E domains which tentatively could be assigned to the αC regions. However, the majority of molecules do not display these structures and additional experiments using the extremely sharp tips are needed to visualize these elusive objects.

Modeling of AFM Images of Fibrinogen Molecules. Since the invention of AFM, the precision of this technique in the visualization of surface structures and different objects on a substrate remains problematic due to overestimations of their real sizes. The image features reproducing the nanoscale objects such as fibrinogen molecules are obtained as a result of the nonlinear force interactions between an object and the probe which has a tip radius of 10−20 nm. The reconstruction of true object dimensions from AFM images has been developed using the mathematical morphology approach with dilation and erosion as the main functions.[28,49] Marchant et al. have applied the

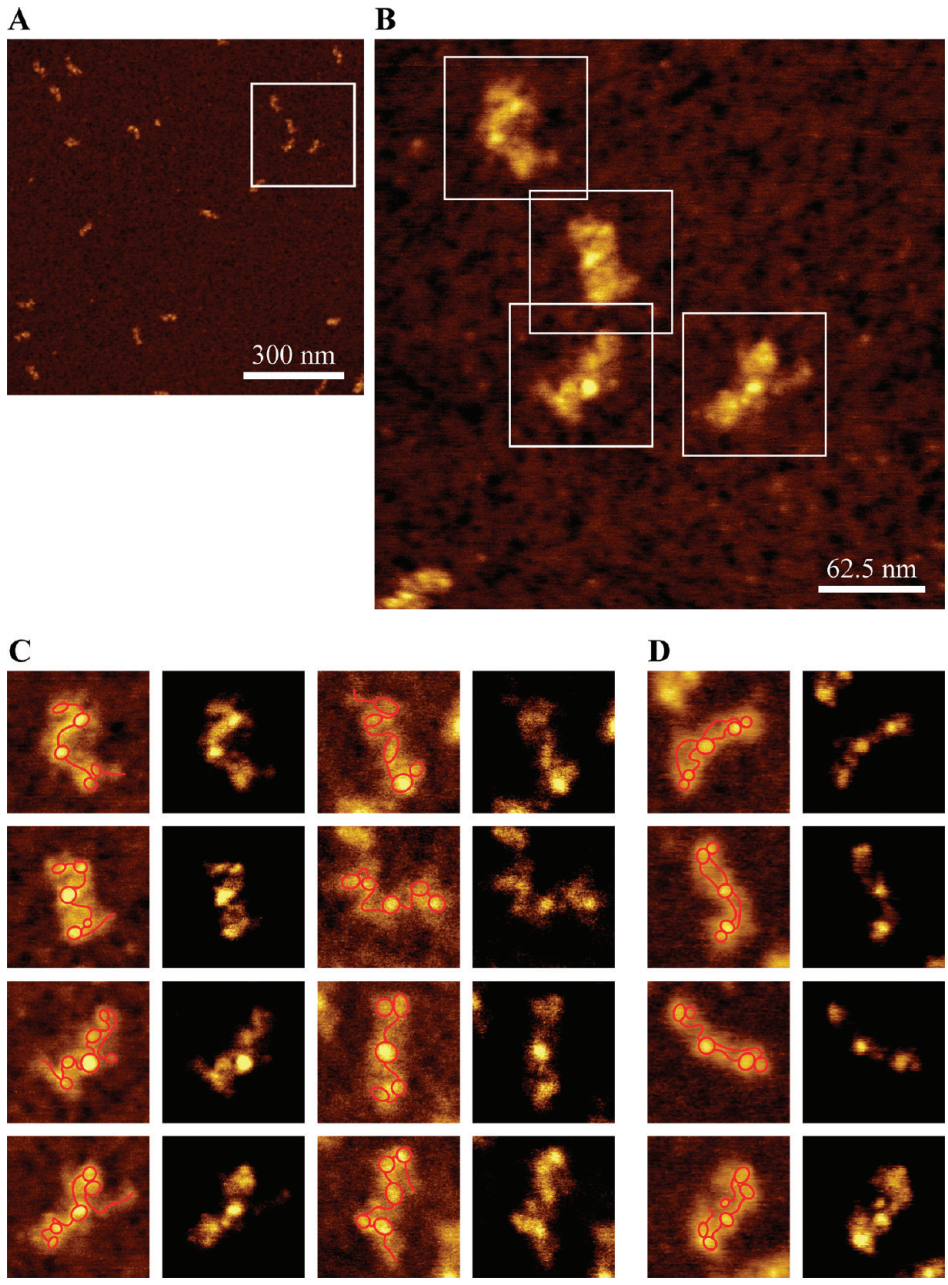

Figure 3. High-resolution images of the fibrinogen molecules. (A) Topography images of a colony of the fibrinogen molecules selected for high-resolution snapshots. The images were obtained in the AM mode. (B) The images taken from a boxed area in panel A. The contrast covers the height corrugations in the range of 0−1.2 nm and 0.4−1.2 nm in panels A and B, respectively. (C) High-resolution snapshots of eight fibrinogen molecules. Four snapshots in the first left column were taken from the boxed areas marked in panel B. High-contrast patterns of each snapshot were generated by the removal of the background and are shown in the second column from the left. Four snapshots from another high-resolution image and their high-contrast patterns are presented in the third and fourth columns from the left, respectively. (D) High-resolution snapshots of four fibrinogen molecules obtained in the FM mode and their respective high-contrast patterns.

dilation procedure to the AFM images of fibrinogen using a sharp probe whose dimensions were deduced from calibrated gold spheres.[32] As expected, the results revealed a substantial overestimation of the molecular width. This reconstruction is a pure mathematical procedure based on the geometrical parameters where the tip-force related effects, which can influence the images, are not accounted for. We have attempted to perform computer modeling of the AFM images of fibrinogen using a program that takes into consideration the tip−sample force interactions.[43] The model used in our studies was based on the recent X-ray study of human fibrinogen[11] (Figure 4A) as well as on the dimensions and structural organization of molecules seen in the high-resolution TEM micrographs.[7−10] The resulting model shown in Figure 4B was used for the presentation of molecules in different conformations most common for fibrinogen adsorbed on mica (Figure 4C). Our initial attempts to obtain images at different levels of tip−sample forces have indicated no noticeable force effects. One possible explanation for the absence of force effects is that the elastic modulus of fibrinogen adsorbed on mica is higher than could be predicted from the measurements of the elastic modulus of protofibrils (4 MPa).[28,50] Indeed, the effective modulus of soft nanoscale objects deposited onto rigid substrates such as mica (elastic modulus ∼60 GPa) might be substantially enhanced, especially when these objects are only of ∼1−2 nm in height.[51] Our attempts to increase the force led to the removal of molecules from the surface by the tip, apparently due to their insufficient adhesion to mica.

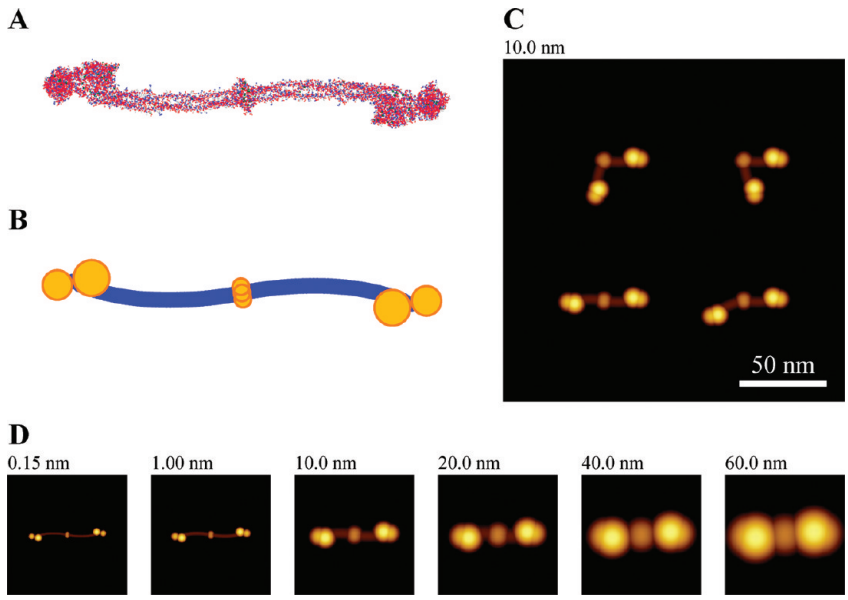

Figure 4. Simulation of the AFM images of the fibrinogen molecules. (A) The 3D structure of fibrinogen based on its crystal structure.[11] (B) The model used in the simulation analyses. (C) The application of the eight-sphere model for the presentation of the most probable conformations observed in the images shown in Figure 2: 106° (top left), 75° (top right), 180° (bottom left), and 157° (bottom right). (D) Computer simulation of the AFM images of single fibrinogen molecules using probes with the tip radii in the 0.15−60 nm range.

Because the tip−sample force effects were not observed in our experiments, we limited our analyses to the geometrical convolution. The computer simulation of AFM images of single fibrinogen molecules on mica was performed for the probes with a tip radii (r) in the 0.15−60 nm range (Figure 4D). The smallest tip ($r = 0.15$ nm) simulates a single-atom tip, whereas the tips with $r \geq 1$ nm relate to the more practically relevant cases. The sharpest probes have radii in the 1−3 nm range, whereas the regular Si probes, which were applied in our studies, are characterized by a tip radius in the 10−20 nm range. The simulations were performed in AM mode with minimal tip−sample force involved ($\ll$1 pN). For $r = 0.15$ nm, the changes in the AFM pattern representing the individual fibrinogen molecules are related to the convolution of the tip with submolecular features (Figure 4D, left panel). The changes in the molecular shape and dimensions were still small when a 1 nm probe was applied. A substantial thickening of the molecular pattern and its transition to a trinodular shape occurred when probes with a tip radius 10 nm and higher were used. The submolecular features became smeared and the thickened patterns were comparable to those observed in our experiments (Figure 2). Therefore, it is reasonable to assume that the structure of fibrinogen molecules adsorbed on mica is similar to that visualized previously in the TEM studies and reconstructed from the X-ray data.

Imaging of Fibrinogen in Liquid and Humid Environment. AFM studies of biological samples can be conducted not only in air but also in humid and liquid environments. This is a unique capability of this microscopic technique, especially when combined with high-resolution visualization of molecular species. Although AFM imaging in liquid is more challenging than in air, these measurements are invaluable for biological objects. The comparison of the geometry, conformation and fine structure of fibrinogen in air and buffer may clarify the effect of hydration. To date, the measurements of fibrinogen in buffer were less frequent than in air. This might be the reason that currently there is no a model explaining how hydration influences the fibrinogen molecules. For example, the observation of fibrinogen oligomers on a hydrophobic substrate in phosphate buffer revealed a change in the molecular shape to overlapping ellipsoids.[27] The topography measurements showed that the height of these objects was ~1.3 nm, suggesting that hydration did not change the molecule's height. In contrast, the measurements of the fibrinogen molecules in phosphate buffer on poly-L-lysine-modified mica revealed much larger heights of ~4 nm.[34] The contour length of the molecules (>60 nm) was also larger than that in dry atmosphere.

The AFM images of fibrinogen on mica in the buffer are shown in Figure 5A. Many observed features can be assigned to single molecules, and several molecular aggregates are seen at the bottom of the image. The length of individual molecules increased slightly, up to ~50 nm compared to their length in air. The length and height of the fibrinogen D and E regions measured in the buffer and in air are presented in Table 1. The results demonstrate that the average height of the D regions (3.7 ± 0.9 nm) is larger than that of the E regions (2.9 ± 0.6 nm), and these heights are ~3 times greater than those measured in dry environment.

A different effect was observed when the fibrinogen molecules on mica were initially dried and then subjected to humid air. It has been previously shown that, under these conditions, a 2 nm water layer covers the mica surface.[52] Imaging in humid air was conducted in FM mode continuously for over 24 h at 22 °C. The images in Figure 5B were taken at the same location before and 6 h after the sample was subjected to humidity at RH > 90%. Changes in the molecular structure caused by humidity were clearly detected (Figure 5C). The molecules gradually spread on the surface and the average height decreased from ~1 to 0.4 nm. Furthermore, at some locations, there were changes in the molecular conformation and small lateral translations of molecules relative to each other. These structural transformations can be expected because under similar conditions, the 2D self-assembly of polypeptides adsorbed on mica has been documented with AFM.[53]

Morphology and Superstructure of Fibrin Fibers. The initial steps of fibrin polymerization and fibrin network formation on graphite have been previously examined using AFM.[29,37] These studies have demonstrated that fibrin monomers initially

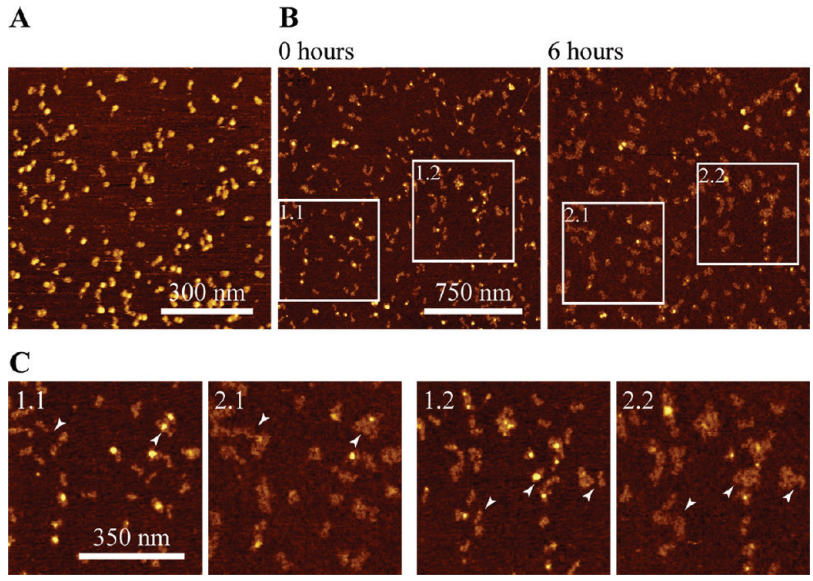

Figure 5. Imaging of fibrinogen in liquid and humid environments. (A) Topography images of the fibrinogen molecules on mica recorded in PBS. (B) Topography images of the fibrinogen molecules on mica in humid air (RH > 95%) taken immediately after the humidity was raised (0 h) and after 6 h. The contrast covers the height corrugations in the range of 0−8 and 0−1.3 nm for panels A and B, respectively. The height of 18 selected molecules was monitored during the time course in two experiments. (C) Enlarged images of the boxed areas shown in panel B.

Table 1. Data Analysis of the AFM Images of Single Fibrinogen Molecules

method	D region[a] (height, nm)	E region[a] (height, nm)
AM in liquid	3.7 ± 0.9	2.9 ± 0.6
FM in air	1.0 ± 0.1	0.9 ± 0.1
AM in air	1.1 ± 0.3	0.7 ± 0.1

[a] The measurements in air were performed for 400 and 72 molecules in the AM and FM modes, respectively. The measurements in buffer were performed for 133 molecules using the AM mode.

assembled into short strands (protofibrils) of 130−200 nm in length. They further propagated until they contacted their neighbors, followed by branching, overlapping and the gradual network formation. The high-resolution AFM images of individual fibrin strands revealed the periodic globular domains with an average spacing of 22.5 nm.[29] Others presented AFM images of fibers formed on mica and glass,[19,36,39] however, no distinctive banding pattern was observed.

We examined the morphology of the fibrillar network, which is assembled from fibrin monomers on mica at the relatively early stages. The samples with a moderate network formation were most suitable for AFM measurements of the fiber dimensions and their nanoscale structure. The AFM visualization of the network deposits on mica showed that they consist of fibrillar aggregates sparsely covering the substrate, with a large number of separate individual fibers. A high-density AFM image of the fibrin network, which is surrounded by numerous individual fibers, is shown in Figure 6A. Determination of the dimensional parameters for individual fibers demonstrated that the variation in the fiber width was from 20 nm to 1 μm. The average height of the fibers was in the 5−30 nm range. On the basis of a width/height ratio, the fibers can be divided into two well-defined groups (the histogram of the distribution of aspect ratios is shown in Figure S1 in the Supporting Information). The fibers in the first group are characterized by an average height of 10 ± 5 nm and aspect ratio of 26 ± 10. The second group includes the fibers with an average height of 23 ± 10 nm and aspect ratio of 12 ± 5. Therefore, the majority of fibers actually look like flat ribbons. This is in contrast to images obtained by SEM and electron microscopy of freeze-dried, shadowed specimens that show seemingly cylindrical fibers.[54−56] Moreover, a nearly cylindrical cross section of the fibers was observed in TEM images.[39,57] It should be noted that AFM allows us to visualize only those objects that lie on the surface as opposed to SEM that allows the visualization of fibers formed in solution. We cannot rule out that the attachment of fibers to mica may induce their flattening or that proximity of the surface may modify the pattern of polymerization.

The fine structure of fibers was revealed at higher magnification. Since the image in Figure 6A covers a surface of 20 × 20 μm^2 and is formed by an array of 4096 × 4096 pixels, a digital zoom of the smaller areas provided micrographs with sufficient data points to visualize the nanometer-scale structural features. Several such small areas are boxed in Figure 6A and their enlarged patterns are presented in the micrographs in Figure 6B−H. Figure 6B−D and F show the parts of fibers that were assigned to the first group. The surfaces of these fibers exhibit a well-defined granular structure with individual grains of ∼10 nm. The grains are arranged in regular patterns with a period of 24.0 ± 1.6 nm along the fiber main axis. The analysis of periodicity of several areas on the surface of a representative fiber using Fast Fourier Transform is shown in Figure S2A−C in the Supporting Information. The average height alternation of ∼1 nm is the distinctive feature of the fibers' surface. The topography profiles along the fibers are rather complex and most likely reflect the submolecular structure which is difficult to decipher due to a tip convolution. The examples of such profiles are shown in Figure S2D in the Supporting Information.

Regularities of the surface corrugations are less pronounced for fibers in the second group and their surfaces have a chenille-like appearance (Figure 6G and H). Furthermore, the axial periodical features are barely distinguishable on the surface of the larger fibers (Figure 7A,B). However, some regular structures with a period close to 23 nm can occasionally be observed in the high-force AFM phase images. At high forces, as the AFM tip penetrates or depresses a soft top layer, it reveals the periodical structure of the fiber's core which becomes visible on phase images. The comparison between the topography of fibers obtained at low and high forces, as well as their phase images, are shown in Figure 7C and D. Similar differences

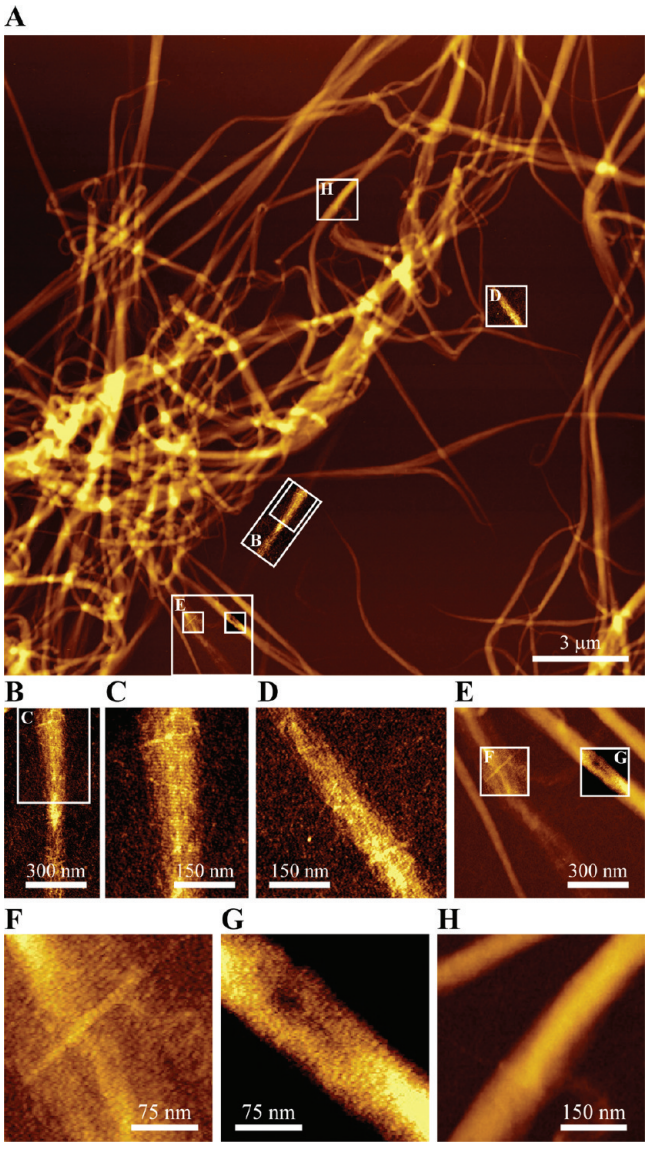

Figure 6. Morphology of fibrin fibers. (A) High-density topography image (4096 × 4096 pixels) of the fibrin network. The contrast covers the height corrugations in the 0−100 nm range. The image has been recorded in a low-force imaging AC mode in air using a soft probe in order to resolve the individual nanoscale grains. (B, C) Topography images of the fiber made by zooming of the boxed areas B in panel A. Contrast covers the height variations in the 0−8 nm range. (D) Topography image of the fiber made by zooming of area D in panel A. (E) The topography images of two fibers (F) and (G) obtained by zooming of area E in panel A. Contrast covers the height variations in the 0−55 (E), 0−22 (F), and 0−12.5 nm (G) ranges. (H) Topography image of the fiber made by zooming of area H in panel A.

between the AFM images obtained at low and high forces have been previously reported for oriented polymers[58] and were explained by stiffness variations due to the regularity in packing of the polymer chains.

Our finding of the periodic 24.0 ± 1.6 nm patterns on the surface of thin fibers should be considered in connection with numerous electron microscopy and diffraction studies, which observed a similar repeat in the fibrin samples prepared by different methods. A periodic cross-striation was first observed in fibrin shadowed by the evaporation of metals.[59] The ridges on the surface of fibers were interpreted as regions of different densities, although the overall resolution of this technique was poor. In contrast, the micrographs of negatively contrasted fibrin,

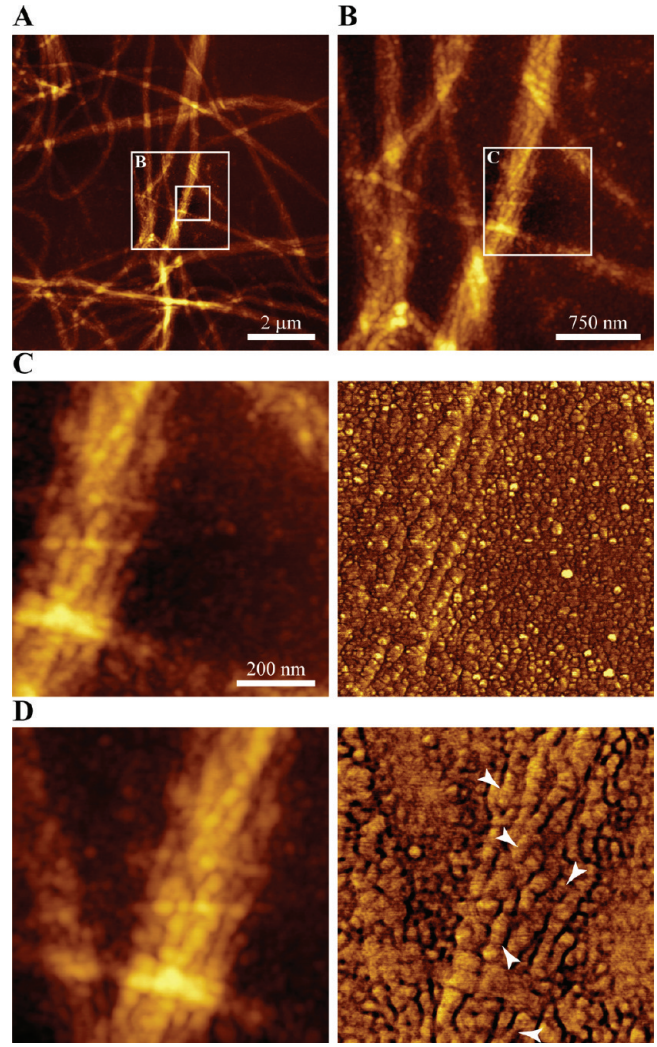

Figure 7. Morphology of thick fibers visualized at low and high forces. (A) Topography images of fibers obtained in the AM mode. (B) The image taken from the boxed area in A. (C) Topography (left panel) and phase contrast (right panel) images obtained at the location shown as a boxed area in (B) using a low-force AM mode display no periodical structures. (D) Topography (left panel) and phase contrast (right panel) AFM images of the same area taken using a high-force AM mode reveal periodical ~23 nm patterns (arrowheads). The contrast covers the height corrugations in the range of 0−30 (A) and 0−20 nm (B, C, D).

which also display a pattern representing the mass distribution along the fiber, produced a detailed pattern: within each 22.5 nm repeat there is one bright stain-excluding band and three narrow light bands, which reflect the packing of fibrinogen domain within protofibrils and their lateral interactions.[4] However, despite the improved resolution of negatively stained fibrin, the micrographs are perceived flat and do not provide information about the "texture" of the surface. Our AFM images, on the other hand, show a furrowed character of the fibrin surface. Based on the previous interpretation of negatively stained fibrin,[5,60] the axial ridges observed in the AFM images of a fiber appear to be formed by the juxtaposition of the D region of two molecules in one strand of a protofibril with the E region of a neighboring molecule in the second strand. The structural order observed in TEM micrographs has been previously supported by studies using small-angle X-ray scattering that allowed measurements of native, hydrated fibrin films and revealed the patterns with a spacing of 22.5 nm and higher order.[3,17]

The observation that periodic corrugations on the surface of thin fibers are smoothed out in larger fibers can not be practically obtained by TEM and X-ray techniques. This transition suggests that the molecular packing inside fibers may be tighter and more regular than that on their surface. This model would be consistent with an earlier proposal[39,61] that the fiber is denser in the center than on the outside. Using AFM-based lateral force manipulation, Guthold et al.[39] have found that the rupture force, F_R, of individual fibrin fibers increased as $F_R \sim D^{1.3}$, where D is the diameter of the fiber. Moreover, the fluorescence intensity, I, of fibrin fibers increased as $I \sim D^{1.3}$. Based on these findings, it has been proposed that the number of molecules per fiber cross section, N, increases as $N \sim D^{1.3}$, which would be consistent with the idea that a fiber has no solid cross section. Should a fiber have a solid cross section, then N would increase as D.[2] This, in turn, would imply that the density of fibers varies as $D^{-0.7}$, that is, the density decreases with increasing diameter. Recent measurements of the elastic modulus of fibrin fibers have demonstrated a similar trend of decreasing modulus with increasing diameter, suggesting that the core of fibrin fibers is denser than the periphery.[61] The regular packing inside the fibers and relatively poor packing on the surface of thick fibers observed in our AFM images supports this conclusion.

Conclusions

A full strength of AFM and especially its environmental capabilities were applied in the present study to generate high-resolution images of fibrinogen molecules and fibrin fibers. The results reveal new details about molecular architecture of these important biological objects. The conformational analysis of the fibrinogen molecules on mica showed the two most energetically favorable conformations. The submolecular features attributed to the subdomains in the D region of the molecule have been visualized in AFM images for the first time. The interplay between the experimental images of fibrinogen molecules and their computer simulated patterns show that the AFM patterns are in good agreement with the molecular dimensions detected by other methods when tip-size effects are taken into account. The experiments in different environments support the expected hydration of the fibrinogen molecules in buffer, whereas the imaging in humid air suggests the 2D spreading of fibrinogen on mica induced by an adsorbed water layer.

Novel structural information has been obtained in AFM studies of fibrin fibers. The regular corrugations with an axial period of 24.0 ± 1.6 nm were visualized on the surface of thin fibrin fibers. This axial spacing has not been previously detected by AFM and is in excellent agreement with a pattern obtained with electron microscopy and small-angle X-ray diffraction. The patterns on the surface of fibers are built from nanoscale grains that are packed with periodical height variations of $\sim$1 nm. This order is less discernible as the fibers become larger which suggests that the molecule packing becomes less regular with the fiber's growth. These transitions appear to present the intermediate steps in the development of mature fibers and fibrillar network.

Acknowledgment. This work was supported by grants from the NIH (T.P.U.) and the American Heart Association (I.S.Y.).

Supporting Information Available. A histogram of the distribution of aspect (width/height) ratios. High-density topography image of a thin fiber, Fourier Transform of height corrugations and topography cross sections. This material is available free of charge via the Internet at http://pubs.acs.org.

References and Notes

(1) Hall, C. E. *J. Biol. Chem.* **1949**, *179*, 857–865.
(2) Hall, C. E.; Slayter, H. S. *J. Biophys. Biochem. Cytol.* **1959**, *5*, 11–17.
(3) Stryer, L.; Cohen, C.; Landridge, R. *Nature* **1961**, *197*, 793–794.
(4) Weisel, J. W.; Warren, S. G.; Cohen, C. *J. Mol. Biol.* **1978**, *126*, 159–183.
(5) Weisel, J. W.; Phillips, G. N.; Cohen, C. *Nature* **1981**, *289*, 263–267.
(6) Fowler, W. E.; Hantgan, R. R.; Hermans, J.; Erickson, H. P. *Proc. Natl. Acad. Sci. U.S.A.* **1981**, *78*, 4872–4876.
(7) Williams, R. C. *Proc. Natl. Acad. Sci. U.S.A.* **1983**, *80*, 1570–1573.
(8) Fowler, W. E.; Erickson, H. P. *J. Mol. Biol.* **1979**, *134*, 241–249.
(9) Williams, R. C. *J. Mol. Biol.* **1981**, *150*, 399–408.
(10) Slayter, H. S. *Ann. N.Y. Acad. Sci.* **1983**, *408*, 131–145.
(11) Kollman, J. M.; Pandi, L.; Sawaya, M. R.; Riley, M.; Doolittle, R. F. *Biochemistry* **2009**, *48*, 3877–3886.
(12) Mosesson, M. W.; Hainfeld, J.; Wall, J.; Haschemeyer, R. H. *J. Mol. Biol.* **1981**, *153*, 695–718.
(13) Erickson, H. P.; Fowler, W. E. *Ann. N.Y. Acad. Sci.* **1983**, *408*, 146–163.
(14) Veklich, Y. I.; Gorkun, O. V.; Medved, L. V.; Nieuwenhuizen, W.; Weisel, J. W. *J. Biol. Chem.* **1993**, *268*, 13577–13585.
(15) Medved, L. V.; Ugarova, T. P.; Veklich, Y. I.; Lukinova, N. I.; Weisel, J. W. *J. Mol. Biol.* **1990**, *216*, 503–509.
(16) Hantgan, R. R.; Fowler, W. E.; Erickson, H. P.; Hermans, J. *Thromb. Haemostasis* **1980**, *44*, 119–124.
(17) Mueller, M. F.; Ferry, J. D.; Lin, J. S. *Biopolymers* **1989**, *28*, 1011–1018.
(18) Brown, A. E. X.; Litvinov, R. I.; Discher, D. E.; Purohit, P. K.; Weisel, J. W. *Science* **2009**, *325*, 741–744.
(19) Drake, B.; Prater, C. B.; Weisenhorn, A. L.; Gould, S. A. C.; Albreht, T. R.; Quate, C. F.; Cannell, D. S.; Hansma, H. G.; Hansma, P. K. *Science* **1989**, *243*, 1586–1589.
(20) Wigren, R.; Ewings, H.; Erlandsson, R.; Welin, S.; Lundstroem, I. *FEBS Lett.* **1991**, *280*, 225–228.
(21) Yung, S.-Y.; Lim, S.-M.; Albertorio, F.; Kim, G.; Gurau, M. C.; Yang, R. D.; Holden, M. A.; Cremer, P. S. *J. Am. Chem. Soc.* **2003**, *125*, 12782–12786.
(22) Cacciafesta, P.; Humphris, A. D. L.; Jandt, K. D.; Miles, M. J. *Langmuir* **2000**, *16*, 8167–8175.
(23) Holland, N. B.; Marchant, R. E. *J. Biomed. Mater. Res.* **2000**, *51*, 307–315.
(24) Gettens, R. T. T.; Gilbert, J. L. *J. Biomed. Mater. Res.* **2006**, *81A*, 465–473.
(25) Marchin, K. L.; Berrie, C. L. *Langmuir* **2003**, *19*, 9883–9888.
(26) Agnihotri, A.; Siedlecki, C. A. *Langmuir* **2004**, *20*, 8846–8852.
(27) Sit, P. S.; Marchant, R. E. *Thromb. Haemostasis* **1999**, *82*, 1053–1060.
(28) Villarubia, J. S. *Surf. Sci.* **1994**, *321*, 287–300.
(29) Marchant, R. E.; Kang, I.; Sit, P. S.; Zhou, Y.; Todd, B. A.; Eppell, S. J.; Lee, I. *Curr. Protein Pept. Sci.* **2002**, *3*, 249–274.
(30) Ishizaki, T.; Saito, N.; Sato, Y.; Takai, O. *Surf. Sci.* **2007**, *601*, 3861–3865.
(31) Toscano, A.; Santore, M. M. *Langmuir* **2006**, *22*, 2588–2597.
(32) Marchant, R. E.; Barb, M. D.; Shainoff, J. R.; Eppell, S. J.; Wilson, D. L.; Siedlecki, C. A. *Thromb. Res.* **1997**, *77*, 1048–1051.
(33) Van De Keere, I.; Willaert, R.; Hubin, A.; Vereecken, J. *Langmuir* **2008**, *24*, 1844–1852.
(34) Taatjes, D. J.; Quinn, A. S.; Jenny, R. J.; Hale, P.; Bovill, E. G.; McDonagh, J. *Cell Biol. Int.* **1997**, *21*, 715–726.
(35) Vikinge, T. P.; Hansson, K. M.; Benesch, J.; Johansen, K.; Ranby, M.; Lindahl, T. L.; Liedberg, B.; Lundstrom, I.; Tengvall, P. *J. Biomed. Oprtics* **2000**, *5*, 51–55.
(36) Blink, A.; Magdic, J.; Fric, J.; Mucevic, I. *Fibrinolysis Proteolysis* **2000**, *14*, 288–299.
(37) Sit, P. S.; Marchant, R. E. *Surf. Sci.* **2001**, *491*, 421–432.
(38) Chtcheglova, L. Ph.D. Thesis, EPFL, Lausanne, 2004, Chapter 4.3
(39) Guthold, M.; Liu, W.; Stephens, B.; Lord, S. T.; Hantgan, R. R.; Erie, D. A.; Taylor, R. M.; Superfine, R. *Biophys. J.* **2004**, *87*, 4226–4236.
(40) Guthold, M.; Liu, W.; Sparks, E. A.; Jawerth, L. M.; Peng, L.; Falvo, M.; Superfine, R.; Hantgan, R. R.; Lord, S. T. *Cell Biochem. Biophys.* **2007**, *49*, 165–181.
(41) Belitser, V. A.; Pozdnjakova, T. M.; Ugarova, T. P. *Thromb. Res.* **1980**, *19*, 807–814.
(42) Magonov, S. N.; Yerina, N. A. *Langmuir* **2003**, *19*, 500–504.
(43) Belikov, S.; Magonov, S. N. *Proc. Am. Control Soc.* **2009**, 979–984.
(44) Krylov, N.; Bogoliubov, N. *Introduction to Non-Linear Mechanics*; University Press: Princeton, 1949.

(45) Belikov, S.; Magonov, S. N. *Proc. Am. Control Soc.* **2010**, 5745–5750.
(46) Fowler, W. E.; Fretto, L. J.; Erickson, L. A.; McKee, P. A. *J. Clin. Invest.* **1980**, *66*, 50–56.
(47) Weisel, J. W.; Veklich, Y.; Gorkun, O. *J. Mol. Biol.* **1993**, *232*, 285–297.
(48) Weisel, J. W.; Stauffacher, C. V.; Bullitt, E.; Cohen, C. *Science* **1985**, *230*, 1388–1391.
(49) Wilson, D. L.; Dalal, P.; Kump, K. S.; Benard, W.; Xue, P.; Marchant, R. E.; Eppell, S. J. *J. Vac. Sci. Technol., B* **1996**, *14*, 2407–2416.
(50) Storm, C.; Pastore, J.; MacKintosh, F. C.; Lubensky, T. C.; Janmey, P. A. *Nature* **2005**, *435*, 191–194.
(51) Domke, J.; Radmacher, M. *Langmuir* **1998**, *14*, 3320–3325.
(52) Beaghole, D.; Radlinska, E. Z.; Ninham, B. W.; Christenson, H. K. *Phys. Rev. Lett.* **1991**, *113*, 8795–8799.
(53) Li, H.; Zhang, F.; Zhang, Y.; ye, M.; Zhou, B.; Tang, Y.-Z.; Yang, H.-J.; Xie, M.-Y.; Chen, C.-F.; He, J.-H.; Fang, H.-P.; Hu, J. *J. Phys. Chem.* **2009**, *113*, 8795–9799.
(54) Weisel, J. W.; Nagaswami, C.; Makowski, L. *Proc. Natl. Acad. Sci. U.S.A* **1987**, *84*, 8991–8995.
(55) Weisel, J. W.; Nagaswami, C. *Biophys. J.* **1992**, *63*, 111–128.
(56) Collet, J. P.; Woodhead, J. L.; Soriano, S. G.; Soria, C.; Mirshahi, M.; Caen, J. P.; Weisel, J. W. *Biophys. J.* **1996**, *70*, 500–510.
(57) Voter, W. A.; Lucaveche, C.; Blaurock, A. E.; Erickson, L. A. *Biopolymers* **1986**, *25*, 2359–2373.
(58) Magonov, S. N. *Encyclopedia of Analytical Chemistry*; John Willey and Sons, Ltd.: Chichester, 2000; pp 7432−7491.
(59) Van Zandt Hawn, C.; Porter, K. R. *J. Exp. Med* **1947**, *86*, 285–292.
(60) Weisel, J. W.; Phillips, G. N.; Cohen, C. *Ann. N.Y. Acad. Sci.* **1983**, *408*, 367–379.
(61) Liu, W.; Carlisle, C. R.; Sparks, E. A.; Guthold, M. *J. Thromb. Haemostasis* **2010**, *8*, 1030–1036.

BM101122G